

Dynamical Taxonomy: some taxonomic ranks to systematically classify every chaotic attractor

Christophe Letellier

Rouen Normandie University — CORIA, Campus Universitaire du Madrillet, F-76800 Saint-Etienne du Rouvray, France
christophe.letellier@coria.fr

Nataliya Stankevich

Laboratory of Topological Methods in Dynamics, National Research University Higher School of Economics, Bolshaya Pecherskaya str., 25/12, Nizhny Novgorod 603155, Russia
stankevichnv@mail.ru

Otto E. RöSSLer

Division of Theoretical Chemistry, University of Tübingen, D-72076 Tübingen, Germany

Received September 14, 2021(accepted for publication on September 12, 2021)

Characterizing accurately chaotic behaviors is not a trivial problem and must allow to determine the properties that two given chaotic invariant sets share or not. The underlying problem is the classification of chaotic regimes, and their labelling. Addressing these problems corresponds to the development of a dynamical taxonomy, exhibiting the key properties discriminating the variety of chaotic behaviors discussed in the abundant literature. Starting from the hierarchy of chaos initially proposed by one of us, we systematized the description of chaotic regimes observed in three- and four-dimensional spaces, which cover a large variety of known (and less known) examples of chaos. Starting with the spectrum of Lyapunov exponents as the first taxonomic ranks, we extended the description to higher ranks with some concepts inherited from topology (bounding torus, surface of section, first-return map, ...).

By treating extensively the RöSSLer and the Lorenz attractors, we extended the description of branched manifold — the highest known taxonomic rank for classifying chaotic attractor — by a linking matrix (or linker) to multi-component attractors (bounded by a torus whose genus $g \geq 3$).

Keywords: Chaos, toroidal chaos, hyperchaos, map, topology

1. Introduction

There are various types of deterministic dynamical behavior which can be observed. Their nature strongly depends on the dimension of the state space involved. RöSSLer upended his early program of research in chaos with an attempt at constructing a hierarchy in providing various examples [RöSSLer, 1983]. On the occasion of his 50th birthday, Michael Klein and Gerold Baier proposed a second version, a classification mainly based on the spectrum of Lyapunov exponents [Klein & Baier, 1991]. Thirty years later still, two of us developed an up-dated version of this hierarchy which, in addition to the spectrum of Lyapunov exponents, also employs first-return map or Poincaré section to distinguishing between the different types of chaos

[Letellier & Rössler, 2020]. The present classification is a direct continuation of these initial contributions whereby it is our aim to open up the *chaos taxonomy* even wider. Taxonomy is the science of classification of a given class of objects using a specific methodology. The aim of our taxonomy is to provide a classification of chaotic attractors into different classes allowing to assign each attractor to one of the pre-established classes. We here means a “systematic” classification, that is, the design and utilization of taxonomic ranks to define the different classes. This requires a terminology based on essential properties rationally deduced [Ereshefsky, 2000] that we will here introduce in the context of dynamical system. This should help to better discriminate whether an attractor is actually of a new type or not [Spratt, 2011; Letellier & Aguirre, 2012]. According to this taxonomy, an attractor would be new when it is not equivalent to another one at the deepest rank. A first impression could be that, asking for a deep taxonomic rank could promote claim for new attractor but, most likely, this will be the opposite because it would require a deep analysis (too often lacking) showing that the attractor have an already known topology. In other words, a non-usual shape of attractor is not sufficient for claiming that this is a new one.

We limit ourselves to the case of continuous dynamical systems. This choice is justified by the fact that a first-return map or a surface of section of a continuous dynamical system leads to a discrete map. As already mentioned, the first ingredient for a chaos taxonomy is the number of positive and null Lyapunov exponents the number of negative Lyapunov exponents being irrelevant. Nevertheless, despite their usefulness in determining the dimension, there are also some limitations in only using the spectrum of Lyapunov exponents, as it will be demonstrated with some examples.

In fact, while developing further this taxonomy, it appeared that the Lyapunov exponents are the first taxonomic rank, that is, a not so discriminating level. We therefore inserted in our taxonomy other ingredients, mainly inherited from topology, allowing to refine, step by step, the characterization of chaotic attractors. The subsequent part of this paper is organized as follows. Section 2 briefly introduces the concepts (Lyapunov exponents, bounding tori, first-return maps and branched manifolds) that we will use to fully determine a taxon. Section 3 provides some examples of the various taxa which can be observed in three- and four-dimensional state spaces, respectively. Section 4 gives a full characterization of the Rössler and Lorenz attractors (with an extension of the description of branched manifold by linking matrix). Section 5 gives some conclusions and perspectives to this work.

2. Essential properties for defining taxa

The dynamical taxonomy is here proposed for dynamical systems governed by a set of d ordinary differential equations

$$\dot{\mathbf{x}} = \mathbf{f}(\mathbf{x}) \quad (1)$$

where $\mathbf{x} \in \mathbb{R}^d$ is the state vector and $\mathbf{f}(\mathbf{x})$ is a vector field which can be either fully continuous or with a piecewise linear switch function, for instance. Since every non-autonomous system can be rewritten as an autonomous system [Ménard *et al.*, 2000], there is no need to have special consideration for them.

In a talk offered at the University of Utah in 1978, Otto E. Rössler suggested a “hierarchy theorem” in the following way [Rössler, 1978]:

Theorem 1. *Every further dimension carries a less trivial type of attractor.*

- \mathbb{R}^1 : point attractor
- \mathbb{R}^2 : periodic attractor
- \mathbb{R}^3 : chaotic attractor
- \mathbb{R}^4 : hyperchaotic attractor
- \mathbb{R}^5 : hyper 2 chaotic attractor
- \mathbb{R}^d when $d \rightarrow \infty$ limit attractor with $(d - 2)$ positive Lyapunov exponents.

He also distinguished *minimal* chaos, with a single positive Lyapunov exponent (for $d > 3$), from *maximal* (or full) chaos with $d - 2$ positive Lyapunov exponents [Rössler, 1983]. The number m of positive Lyapunov exponents is indeed an essential property for (roughly) quantifying the degree of chaoticity of a given attractor. Let us designate the m dimensions associated with the m positive Lyapunov exponents by C^m ,

“C” meaning chaotic. Thus C^0 is related to periodic or quasi-periodic behavior, C^1 to chaotic behavior, C^2 to hyperchaos, and so on.

One of the missing ingredients in the theorem 1 is the role played by the oscillating nature of the behavior, that is, by tori. In a d -dimensional state space \mathbb{R}^d , it is possible to embed a torus T^n characterized by the product of $n \leq d-1$ circles. A torus T^{d-1} is the maximal regular structure which can be embedded in a d -dimensional space. By regular, we mean a structure which is not *strange* in the sense of [Ruelle & Takens, 1971], that is, which is neither fractal nor leading to a solution which is sensitive to initial conditions. According to the distinction between *strange* and *chaotic* invariant set introduced by [Grebogi *et al.*, 1984], we prefer to use the term chaotic than strange for non-regular invariant set. In this approach, a point is a torus $T^0 \subset \mathbb{R}^1$ and a limit cycle is a torus $T^1 \subset \mathbb{R}^2$. With the first dimension occurs the notion of *singular point*. With the second dimension emerges the notion of *oscillation*; the solution can be aperiodic (an expanding spiral) in a two-dimensional space, but there is a fundamental property which cannot be fulfilled in that case: recurrence, that is, boundedness. Without it, the solution does not belong to an invariant set and is not further considered here. The present taxonomy is therefore for recurrent solutions in the sense of [Birkhoff, 1927]. In a three-dimensional space, a torus T^2 can be embedded and the corresponding behavior is the so-called quasi-periodic one. Such invariant set is neither strange nor chaotic: it is regular and corresponds to C^0 . It will be designated by C^0T^2 . A torus T^p has p null exponents: they correspond to the second part of the spectrum of Lyapunov exponents which is here used to define a new taxonomic rank. C^0T^1 and C^0T^2 are two different taxa, distinguished by counting the positive and null Lyapunov exponents: they are associated with $(m, p) = (0, 1)$ and $(0, 2)$, respectively.

Minimal chaos is characterized by one positive Lyapunov exponent: it is therefore $C^1T^1 \subset \mathbb{R}^d$ with $d > 3$: chaos is necessarily maximal in \mathbb{R}^3 . Recurrent oscillations are designated by T^1 (one null exponent). A torus T^n is necessarily embedded within a space \mathbb{R}^d with $d \geq n + 1$. In these two cases, the minimal dimension δ in which those solutions can be observed is such as $\delta = m + p + 1$: let us name this minimal dimension, the *dynamical dimension*. Typically, when there is a single negative Lyapunov exponent, this is the dimension d of the system. There is one special case to discuss for which this relationships does not work. In its simplest form, toroidal chaos corresponds to a torus whose surface is stretched and folded as described by [Curry & Yorke, 1978]: it is designated by C^1T^2 and one could expect two null and one positive Lyapunov exponents. Nevertheless, such a toroidal chaos can be produced by a three-dimensional systems for which there is necessarily a negative Lyapunov exponent, imposing $m + p = 2$. In fact, the surface of the torus is not regular since it is stretched and folded: the second null exponent which should be associated with the toroidal surface is therefore degenerated and is “merged” with the positive Lyapunov exponent. Three-dimensional toroidal chaos is therefore characterized by one positive and one null Lyapunov exponents. Such a special case is designated as $C^1T_d^2$, “d” meaning that there are actually $p - 1$ (and not p) null exponents: in this case, one should speak of “degenerated toroidal chaos”. We will show that when produced by a four-dimensional system, such behavior is no longer degenerated and two null Lyapunov exponents are actually found as exemplified with the driven van der Pol system investigated by [Ueda, 1993] in Section 3.

Definition 1. A dynamics is said to be *degenerated* when a null Lyapunov exponent is merged with a positive one.

The first two taxonomic ranks are provided by the integers m and p , respectively.

Definition 2. The chaotic level is maximal when $m = d - 2$ with $d \geq 3$.

Definition 3. The toroidal level is maximal when $p = d - 1$ with $d \geq 2$.

It is thus possible to discriminate some behaviors as follows [Klein & Baier, 1991; Letellier & Rössler, 2020; Stankevich *et al.*, 2020].

C^0T^1	Periodic orbit	C^2T^1	Hyperchaos
C^0T^2	Two-frequency quasi-periodic regime	C^2T^2	Toroidal hyperchaos
C^1T^1	Chaos	C^2T^2	Three-frequency quasiperiodic regime
C^1T^2	Toroidal chaos	...	

A dimension connected to the spectrum of Lyapunov exponents is the Kaplan-Yorke dimension which is defined as follows [Kaplan & Yorke, 1979; Frederickson *et al.*, 1983].

Definition 4. Let $\lambda_1 \geq \lambda_2 \geq \dots \geq \lambda_j \geq \dots \geq \lambda_n$ be the spectrum of ordered Lyapunov exponents and let k be the index such as $\sum_{i=1}^k \lambda_i \geq 0$ and $\sum_{i=1}^{k+1} \lambda_i < 0$. The Kaplan-Yorke dimension is

$$D_{KY} = k + \frac{\sum_{i=1}^k \lambda_i}{|\lambda_{k+1}|}.$$

Property 1. By definition, $k \geq m + p - 1$ for non-degenerated torus, and $k \geq m + p$ otherwise.

Property 2. By definition, a taxon has a Kaplan-Yorke dimension such as $m + p - 1 \leq D_{KY} \leq d$ for non-degenerated cases, and $m + p - 2 \leq D_{KY} \leq d$ otherwise.

It is possible to define the *dynamical* dimension δ as follows.

Definition 5. The *dynamical dimension* δ is such as

$$\delta = \begin{cases} m + p & \text{if degenerated} \\ m + p + 1 & \text{otherwise} \end{cases} \quad (2)$$

and $\delta \leq d$. It corresponds to the minimal number of variables required to observe a given dynamics.

The case of *conjugated dynamics* will be described in Section 3.

There is a simple relationship between the dynamical dimension δ and the Kaplan-Yorke dimension D_{KY} : it reads as

$$\delta = \begin{cases} \text{Int}(D_{KY}) + 1 & \text{for dissipative system} \\ D_{KY} & \text{conservative system.} \end{cases} \quad (3)$$

When there is a single negative Lyapunov exponent, $\delta = d$: in other terms, $\delta = d + 1 - n_n$ where n_n is the number of negative Lyapunov exponents.

Definition 6. The dynamics is maximal when $\delta = d$.

A maximal dynamics actually explores all the dimensions of the state space: it cannot be embedded within a space with a smaller dimension.

Corollary 1. *Dissipative m -chaos $C^m T^1$ is maximal when $m = d - 2$, and is necessarily maximal in a three-dimensional space.*

Characterizing a chaotic attractor using its spectrum of Lyapunov exponents corresponds to the first two taxonomic ranks quantified by m and p , respectively. In the analogy with the taxonomy for classifying animals, these two integers could correspond to the *class* and the *order* (Fig. 1): for instance, the first two taxonomic ranks for red fox is *mammal* and *carnivore*, respectively. The next step would be to frame a little bit more the nature of the chaotic invariant set by providing the “*family*”, the analog of claiming that red fox is a canidae.

For chaotic attractors, there is a concept for that: the bounding tori introduced by [Tsankov & Gilmore, 2003, 2004]. The idea is to bound chaotic invariant set by a torus. The corresponding torus has a genus g defined by the number of its holes. A few examples of bounding tori are provided in Fig. 2. It appears that the genus is not sufficient to distinguish all possible configurations: for instance, we drew the two different bounding tori of genus 5 [Figs. 2(d) and 2(e)]. At least, a second number should be provided as

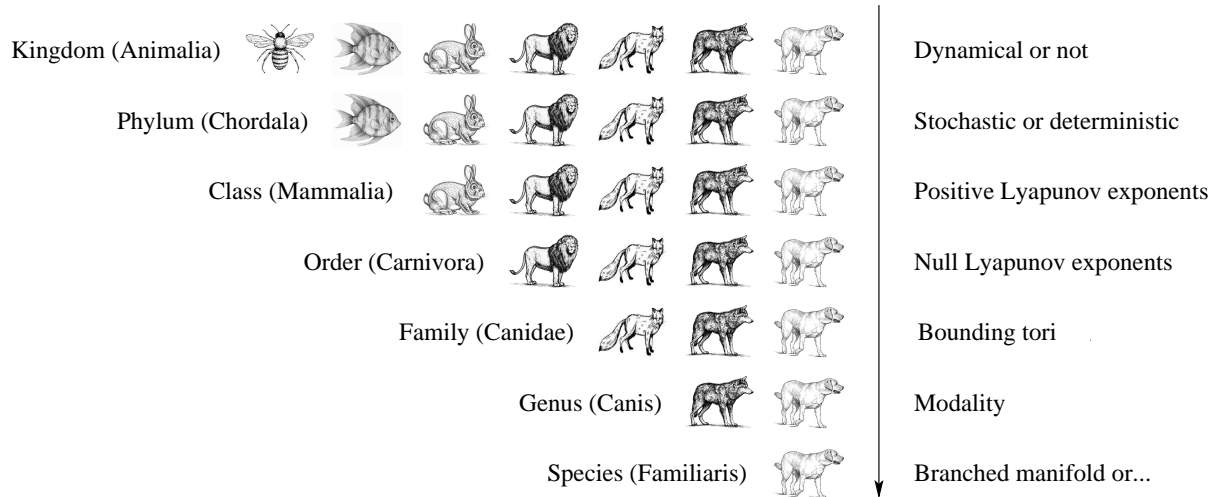


Figure 1. Analogy between the hierarchy of taxonomic ranks as developed for animals and those required for fully describing chaotic attractors. The “modality” corresponds to the number of mixing processes. The highest taxonomic rank is associated with branched manifold for strongly dissipative system whose dynamical dimension is $\delta = 3$.

the number f of focus holes around which the trajectory flows. Thus the two genus-5 bounding tori are characterized by the pairs $(5,3)$ and $(5,4)$, respectively. A more sophisticated and complete labelling can be found in [Tsankov & Gilmore, 2004]. To provide some well-known examples, the spiral Rössler attractor is bounded by the torus $(1,1)$, the Lorenz attractor is bounded by the torus $(3,2)$, the torus $(4,3)$ corresponds to a three-fold cover of the Rössler attractor [Letellier & Gilmore, 2001] and a three-fold cover of the proto-Lorenz attractor [Miranda & Stone, 1993] is bounded by the torus $(4,3)$.

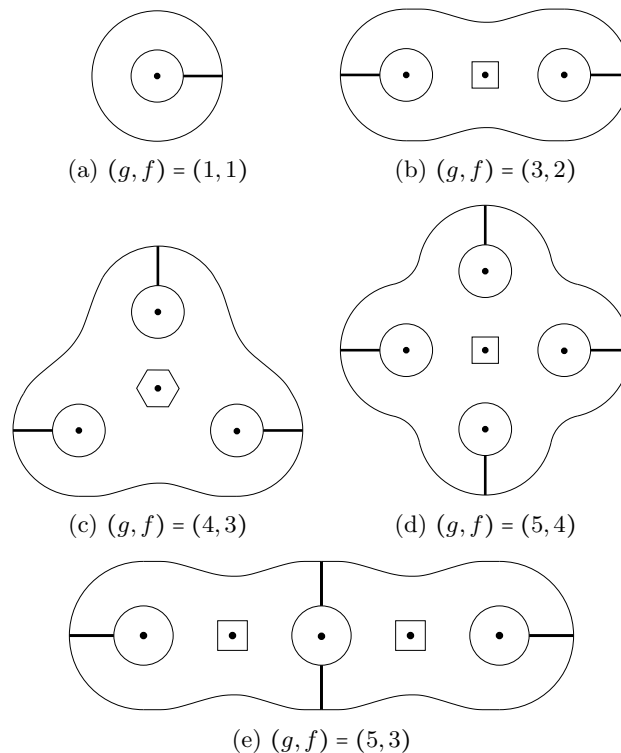


Figure 2. Bounding tori of various genus g ($g \leq 5$). The $g - 1$ components of the Poincaré section are plotted as thick lines. Case (a) applies for the Rössler attractor and (b) for the Lorenz attractor. Cases (c) and (d) may correspond to the 3- and 4-fold covers of the proto-Lorenz system [Miranda & Stone, 1993; Letellier & Gouesbet, 1995]. Case (e) can correspond to a multi-scroll attractor [Aziz-Alaoui, 1999].

Once the genus- g bounding torus is determined, the next step is to compute a first-return map to a $(g - 1)$ -component Poincaré section (when $g > 2$). This means for instance that the Lorenz attractor, which is bounded by a genus-3 torus, must be investigated by using a two-component Poincaré section, leading to a four-branches maps [Letellier *et al.*, 1994; Byrne *et al.*, 2004] as detailed in Section 4. The description of the different types of first-return map is still in its infancy. Rössler started to provide various examples of them [Rössler, 1979a]. The cases of the three possible unimodal maps (Fig. 3) were extensively treated by [Letellier, 2021]. The simplest way to describe a first-return map would be to count the number of critical points (demarcating the monotone branches) or the number of foldings counted in a Poincaré section when it is possible to do so. Describing simply every type of maps is still an open problem, particularly for weakly dissipative systems. Produced by a strongly dissipative system, the spiral Rössler attractor has one critical point associated with a folding [Fig. 2(b)]. The Lorenz attractor has a first-return map to a 2-component Poincaré section characterized by 3 critical points associated with a tearing [Byrne *et al.*, 2004]. Let us here simply use the number n_c of mixing processes which either corresponds to the number of critical points (equal to the number of monotone branches minus one), or the number of foldings counted in the Poincaré section when toroidal chaotic attractor is observed. We name *modality* the number n_c .

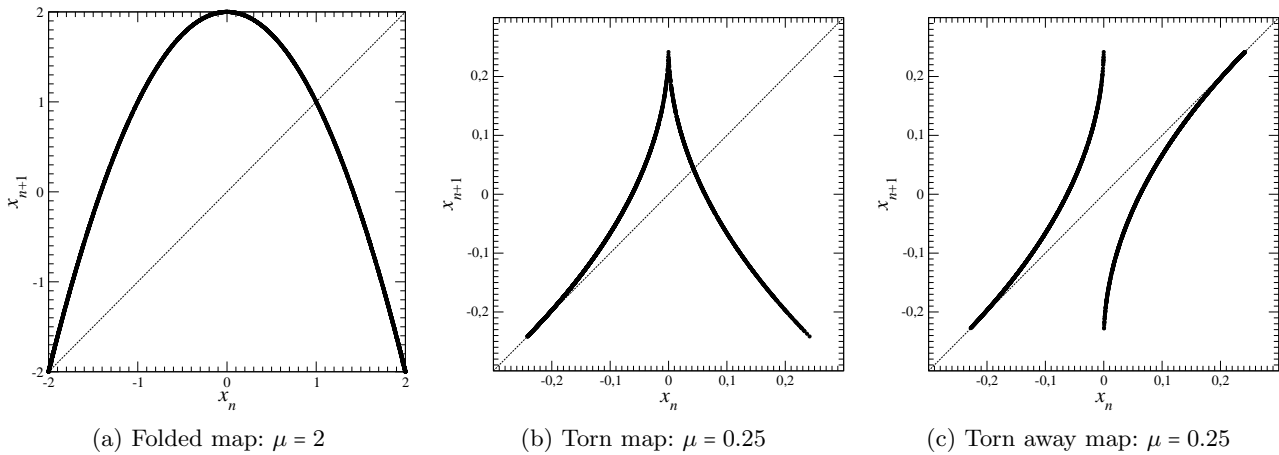


Figure 3. The three possible unimodal maps.

The last taxonomic rank, corresponding to the most selective one, would be, for three-dimensional dissipative systems, a branched manifold [Mindlin & Gilmore, 1992; Tuffillaro *et al.*, 1992; Letellier *et al.*, 1995; Gilmore, 1998]. The simplest branched manifolds associated with the three types of map shown in Fig. 3 are discussed by [Letellier, 2021]. We postpone for future works to provide this last taxonomic rank for all the systems investigated in the next section, the problem being still open for some cases.

Using all these essential properties considered as different taxonomic ranks, a taxon could be described by a set of integers as follows.

- the number m of positive Lyapunov exponents;
- the number p of null Lyapunov exponents;
- the genus g of the bounding torus and its number f of focus holes (Betti numbers could be an efficient way to describe them [Charó *et al.*, 2020, 2021]);
- the modality n_c , that is, the number of critical points or of mixing processes (folding or tearing);
- the last taxonomic rank is not yet sufficiently advanced to be fully summarized by a set of integers. Attractors with a dynamical dimension $\delta = 3$ can be described by a branched manifold [Gilmore, 1998]: when they are bounded by genus-1 torus, they can be described by a $n_c \times n_c$ linking matrix [Tuffillaro *et al.*, 1992; Letellier *et al.*, 1995]. The case of higher genus g tori will be treated in Section 4. More generalized topological description are still to be developed for high-dimensional and/or conservative systems.

Providing these numbers allows to refine each taxon as illustrated in Fig. 1. It is worthy to note that

in most of the literature, the attractors are only described using the first taxonomic ranks, that is, the less discriminating ones. The taxon associated with a given chaotic attractor is fully described only when the last taxonomic rank is determined, that is, when a branched manifold (or some generalized topological description) is provided.

3. Examples of various types of invariant sets

To help the reader to have some intuition with our dynamical taxonomy, we now propose a set of different types of behaviours which can be produced by three- and four-dimensional systems. The invariant sets are plotted with some of their characteristics in Table 1: they are produced by the systems which are reported with the retained parameter values in Table 2. All our examples are such that there is a single negative Lyapunov exponent, in agreement with our assumption that additional negative Lyapunov exponents are irrelevant for the taxonomy of invariant sets. Consequently, the dynamical dimension δ is here equal to the dimension d of the system. Cases (a), (b), (e), (g), (h), and (j) are non-degenerated cases where m (p) is the number of positive (null) Lyapunov exponents. All the invariant sets but cases (c) and (h) are bounded by a trivial genus-1 torus: a single component is therefore required for computing the Poincaré section. Case (a) is a quasi-periodic regime C^0T^2 as revealed by the annular Poincaré section [Table 1(a)] and there is no mixing process ($n_c = 0$): the modality is null. Case (b) is a maximal chaos characterized by a unimodal map ($n_c = 1$) produced by the Rössler system. Case (e) is a toroidal chaos $C^1T^2 \subset \mathbb{R}^4$ produced by the mixed driven van der Pol system with five foldings [they can be counted from the inner part of the Poincaré section as indicated by the red disks in Table 1(e)]: the modality is thus $n_c = 5$. This latter system is mixed because it is made of dissipative van der Pol oscillator driven by a conservative harmonic oscillator [Ménard *et al.*, 2000].

Case (g) is a toroidal chaos $C^1T^2 \subset \mathbb{R}^4$ produced by the conservative Hénon-Heiles system. In such a case, $D_{KY} = 4$. The chaotic sea is bounded by a genus-1 torus [Table 1(g)]; it is possible to refine the bounding of the invariant set by associating tori with the different quasi-periodic islands exhibited in the Poincaré section. There is at least five additional tori, more or less knotted inside the main genus-1 bounding torus, which can be used to bound the chaotic sea. They are relevant to characterize the structure of conservative toroidal chaos [Tricoche *et al.*, 2011]. We therefore suggest to set the modality to $n_c = 5$ for this type of toroidal chaos. According to the procedure developed by [Mangiarotti & Letellier, 2021], this attractor should be characterized by a seven-strip branched manifold but this is out of the scope of the present paper.

Case (j) is the first-example of hyperchaotic chaos $C^2T^1 \subset \mathbb{R}^4$ discussed by [Rössler, 1979b]. The first-return map to the Poincaré section has at least four branches [Table 1(j)]. The presence of a two-dimensional unstable manifold induces a very thick first-return map which makes the partition difficult to establish. Within the scope of this work, we will limit ourselves to state that the modality is $n_c \geq 4$.

Among the five cases remaining to investigate, four are degenerated. Case (c) is a toroidal chaos whose surface is stretched and folded as depicted in the Curry-Yorke scenario [Curry & Yorke, 1978]. Since the surface is stretched, it can no longer be associated with a null Lyapunov exponent but with a positive one. Since the structure is still characterized by an annular structure [Table 1(c)], it should be designated as C^1T^2 . We thus consider that the second null Lyapunov exponent is degenerated and is merged with the positive one. We have $p-1$ null Lyapunov exponents. There is four foldings [see the red disks in Table 1(c)], leading to a modality $n_c = 4$. A six-strip branched manifold should describe the topology of this attractor (postponed for future works).

Case (h) is a nearly conservative toroidal chaos — the averaged trace $\overline{\text{Tr}\mathcal{J}} = -6 \cdot 10^{-5}$ is slightly negative — produced by a mixed four-dimensional system. This is an example of invariant set bounded by a genus-3 torus [see Fig. 2(b)]: a property which results from its inversion symmetry. There is two sets of quasi-periodic islands and, consequently, two inner tori bound the chaotic sea [Table 1(h)]. Compared to the chaotic sea produced by the Hénon-Heiles system [Table 1(g)], it is simpler since it presents a smaller number of quasi-periodic islands: using the conjecture used for the Hénon-Heiles system, the modality would be $n_c = 2$.

Table 1. Invariant sets produced by the dynamical systems here investigated. Are reported for each one: the type C^mT^p , the spectrum of Lyapunov exponents, the Kaplan-Yorke dimension d_{KY} , the dynamical dimension δ , and the number n_c of mixing processes (critical points, foldings). A plane projection and a Poincaré section or a first-return map [cases (b) and (i)] are provided.

	State portrait	Map		State portrait	Map
(a) [1] C^0T^2 $\lambda_1 = 0.0$ $\lambda_2 = 0.0$ $\lambda_3 = -0.0803$ $d_{KY} = 2.0$ $\delta = 3$ $n_c = 0$			(g) [6] C^0T^2 $\lambda_1 = 0.0507$ $\lambda_2 = 0.00$ $\lambda_3 = 0.00$ $\lambda_4 = -0.0507$ $d_{KY} = 4.0$ $\delta = 4$ $n_c \stackrel{?}{=} 4$		
(b) [2] C^1T^1 $\lambda_1 = 0.105$ $\lambda_2 = 0.0$ $\lambda_3 = -3.2779$ $d_{KY} = 2.032$ $\delta = 3$ $n_c = 1$			(h) [7] C^1T^2 $\lambda_1 = 0.06579$ $\lambda_2 = 0.0$ $\lambda_3 = 0.0$ $\lambda_4 = -0.06758$ $d_{KY} = 3.97$ $\delta = 4$ $n_c \stackrel{?}{=} 2$		
(c) [1] $C^1T_d^2$ $\lambda_1 = 0.1408$ $\lambda_2 = 0.0$ $\lambda_3 = -5.1834$ $d_{KY} = 2.0272$ $\delta = 3$ $n_c = 4$			(i) [5] C^1T^3 $\lambda_1 = 0.003$ $\lambda_2 = 0.0$ $\lambda_3 = 0.0$ $\lambda_4 = -0.003$ $d_{KY} = 4.0$ $\delta = 4$ $n_c = ?$		
(d) [3] $C^1T_d^2$ $\lambda_1 = 0.0179$ $\lambda_2 = 0.0$ $\lambda_3 = -0.0179$ $d_{KY} = 3.0$ $\delta = 3$ $n_c = ?$			(j) [8] C^2T^1 $\lambda_1 = 0.115$ $\lambda_2 = 0.021$ $\lambda_3 = 0.0$ $\lambda_4 = -24.931$ $d_{KY} = 3.01$ $\delta = 4$ $n_c \geq 4$		
(e) [4] C^1T^2 $\lambda_1 = 0.5762$ $\lambda_2 = 0.0$ $\lambda_3 = 0.0$ $\lambda_4 = -0.7559$ $d_{KY} = 3.7623$ $\delta = 4$ $n_c = 5$			(k) [9] $C^2T_{cd}^2$ $\lambda_1 = 0.0108$ $\lambda_2 = 0.0005$ $\lambda_3 = 0.0$ $\lambda_4 = -0.138$ $d_{KY} = 3.08$ $\delta = 4$ $n_c = 2$		
(f) [5] $C^1T_c^2$ $\lambda_1 = 0.0088$ $\lambda_2 = 0.0$ $\lambda_3 = 0.0$ $\lambda_4 = -0.0588$ $d_{KY} = 3.1492$ $\delta = 4$ $n_c = 1$					

[1] = [Stankevich *et al.*, 2020], [2] = [Rössler, 1976], [3] = [Sprott, 1997], [4] = [Ueda, 1993], [5] = [Klein & Baier, 1991], [6] = [Hénon & Heiles, 1964], [7] = [Charó *et al.*, 2019], [8] = [Rössler, 1979b], [9] = [Anishchenko & Nikolaev, 2005]

Table 2. Governing equations of the dynamical systems here investigated. Parameter values and initial conditions (IC) when they may be sensitive) are reported.

Reference	Governing equations		
(a) [Stankevich <i>et al.</i> , 2020]	$\dot{x} = y$ $\dot{y} = (\alpha + z + x^2 - \beta x^4) y - \omega_0^2 x$ $\dot{z} = \mu - z - \epsilon y^2$	$\alpha = 1.5$ $\beta = 0.04$ $\mu = 4$ $\epsilon = 0.02$ $\omega_0 = 2\pi$	
(b) [Rössler, 1976]	$\dot{x} = -y - z$ $\dot{y} = x + ay$ $\dot{z} = b + z(x - c)$	$a = 0.43295$ $b = 2$ $c = 4$	
(c) [Stankevich <i>et al.</i> , 2020]	$\dot{x} = y$ $\dot{y} = (\alpha + z + x^2 - \beta x^4) y - \omega_0^2 x$ $\dot{z} = \mu - z - \epsilon y^2$	$\alpha = 9$ $\beta = 0.016$ $\mu = 4$ $\epsilon = 0.02$ $\omega_0 = 2\pi$	
(d) [Sprott, 1997]	$\dot{x} = y$ $\dot{y} = z$ $\dot{z} = a(1 - x^2)x - x^2 y$	$a = 0.027$ $x_0 = 0.98$ $y_0 = 0.58 x_0$ $z_0 = 0$	
(e) [Ueda, 1993]	$\dot{x} = y$ $\dot{y} = \mu(1 - \gamma x^2)y - x^3 + u$ $\dot{u} = v$ $\dot{v} = -\omega^2 u$	$\mu = 0.2$ $x_0 = 0.2$ $\gamma = 8$ $y_0 = 0.2$ $B = 0.35$ $u_0 = B$ $\omega = 1.02$ $v_0 = 0$	
(f) [Klein & Baier, 1991]	$\dot{x} = y$ $\dot{y} = -x - az - bw$ $\dot{z} = d(1 - x^2) - cw$ $\dot{w} = cz - ew$	$a = 0.15$ $x_0 = -0.043$ $b = 0.25$ $y_0 = -0.157$ $c = 0.1$ $z_0 = -3.113$ $d = 0.3922$ $w_0 = -1.826$ $e = 0.05$	
(g) [Hénon & Heiles, 1964]	$\dot{x} = V_x$ $\dot{V}_x = -x - 2xy$ $\dot{y} = V_y$ $\dot{V}_y = -y - x^2 + y^2$	$x_0 = 0$ $y_0 = -0.15$ $V_{x,0} = 0.478$ $V_{y,0} = 0$	
(h) [Charó <i>et al.</i> , 2019]	$\dot{x} = A\pi \sin\left(\pi\left[x^2 u + x - u\right]\right) \sin(\pi y)$ $\dot{y} = A\pi \cos\left(\pi\left[x^2 u + x - u\right]\right) \cos(\pi y)$ $\dot{u} = v$ $\dot{v} = -\omega^2 u$	$A = 0.1$ $x_0 = 0.2$ $\eta = 0.1$ $y_0 = 0$ $\omega = \frac{\pi}{5}$ $u_0 = 0$ $v_0 = \omega \eta$	
(i) [Klein & Baier, 1991]	$\dot{x} = y$ $\dot{y} = -x - z - w$ $\dot{z} = cw$ $\dot{w} = a(1 - x^2) - cz$	$a = 0.03$ $x_0 = 0.6173$ $c = 0.1313$ $y_0 = -0.1368$ $z_0 = -0.0078$ $w_0 = -0.1231$	
(j) [Rössler, 1979b]	$\dot{x} = y + ax + w$ $\dot{y} = -x - z$ $\dot{z} = b + zy$ $\dot{w} = -cz + dw$	$a = 0.25$ $x_0 = -10$ $b = 3$ $y_0 = -6$ $c = 0.5$ $z_0 = 0$ $d = 0.05$ $w_0 = 10.1$	
(k) [Anishchenko & Nikolaev, 2005]	$\dot{x} = -y$ $\dot{y} = x + \mu y - yw - \delta y^3$ $\dot{z} = w$ $\dot{w} = -\beta z - \alpha w + \alpha \Phi(y)$	$\alpha = 0.2$ $\beta = 0.43$ $\delta = 0.001$ $\mu = 0.0809$ $\theta = \frac{\pi}{3}$	

Case (i) is another example of toroidal chaos produced by a conservative system: rather than governed by two frequencies as in the cases (c) and (e), there are three different frequencies involved in the toroidal structure. This is therefore a toroidal chaos $C^1T_d^3 \subset \mathbb{R}^4$. It is degenerated for reasons similar to those

involved in the case (c). The Poincaré section [Table 1(h)] looks like a torus: this is a first-order Poincaré section (as all the other sections discussed in this work) defined as

$$\mathcal{P}_1 \equiv \{(x_n, z_n, w_n) \in \mathbb{R}^3 \mid y_n = 0\}. \quad (4)$$

To exhibit the toroidal nature of this invariant set, a second-order Poincaré section can be used [Parker & Chua, 1989]: it is defined as

$$\mathcal{P}_2 \equiv \{(x_n, z_n) \in \mathbb{R}^2 \mid y_n = 0, |w_n| < \epsilon, \dot{w}_n > 0\} \quad (5)$$

and corresponds to the intersections of the trajectory with the first-order Poincaré section and located in a small domain here defined by the red dashed lines in Table 1(i). The thickness ϵ is set as a compromise between the accuracy of the plot and the time required to compute it: with $\epsilon = 0.04$, to get 32,000 points in \mathcal{P}_2 , we integrated the system over $8.4 \cdot 10^8$ time steps, leading to $6.4 \cdot 10^5$ intersections with \mathcal{P}_1 . An annular shape is clearly revealed by the section \mathcal{P}_2 (Fig. 4). This behavior is degenerated since the torus T^3 is characterized by two null Lyapunov exponents and not three.

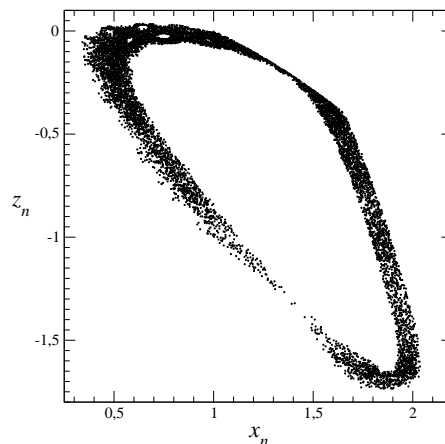
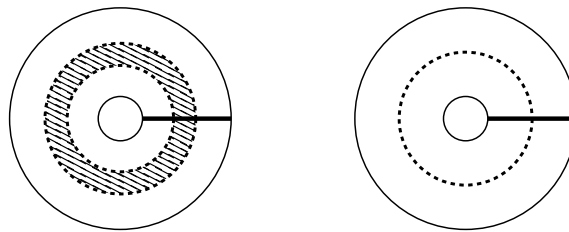


Figure 4. Second-order Poincaré sections \mathcal{P}_1 and \mathcal{P}_2 of the toroidal chaos C^1T^3 produced by the four-dimensional conservative oscillator (i). Same parameter values as reported in Table 2(i) and $\epsilon = 0.04$.

The last degenerated case, system (k), is discussed with the case (f). Let us start with the latter. The Poincaré section has the typical annular structure of a toroidal behavior [Table 1(f)]. Nevertheless, the section looks like a spiral Rössler attractor. In fact, this behavior is observed after a period-doubling cascade in tori when parameter d is varied. Such a route to chaos was reported by [Franceschini, 1983; Kaneko, 1983; Arnéodo *et al.*, 1983; Klein & Baier, 1991; Letellier *et al.*, 2007]. It was shown that such a behaviour can be produced by two conjugated maps [Kaneko, 1986]. The specificity of this toroidal chaos arising after a period-doubling cascade on tori is that it cannot be degenerated in a three-dimensional space. Indeed, to have a “horseshoe map” conjugated to a toroidal structure, it is necessary to have a four-dimensional space, exactly as it is required to have such a space for embedding a Klein bottle [Klein, 1882]. A Klein bottle is a closed, single-sided mathematical surface of genus 2 [Séquin, 2013]: it is the fourth-dimensional version of the three-dimensional Möbius band. It is not possible to construct a Klein surface without self-intersection in a three-dimensional space: the fourth dimension is required for that. For similar reason, it is not possible to get conjugated toroidal chaos CT_c^2 in a three-dimensional space without self-intersection. Conjugated toroidal chaos $C^1T_c^2 \subset \mathbb{R}^4$ is thus structurally different from the toroidal chaos $C^1T_d^2$ or the toroidal chaos C^1T^2 — produced by the oscillator investigated by [Stankevich *et al.*, 2020] and by the driven van der Pol system [Ueda, 1993], respectively — which results from a Curry-Yorke scenario and can be embedded within a three-dimensional space.

Case (k) is quite similar to case (f) but it presents a possibility which is not observed in the system (f): as observed in the Rössler system, after the period-doubling cascade, the attractor is developed up to a homoclinic situation [Letellier *et al.*, 1995; Malykh *et al.*, 2020] where the attractor is bounded with

a torus whose inner radius is null [Fig. 5(b)]. The Poincaré section does no longer present a non-visited domain in its centre. Then the fourth dimension allows a toroidal hyperchaos $C^2T_d^2$ [Table 1(k)].



(a) Just after the period-doubling (b) Homoclinic situation

Figure 5. Bounding tori drawn in a Poincaré section for the conjugated toroidal chaos $C^1T_c^2$ produced by the system (k). (a) Just after the period-doubling cascade in tori, the invariant set is bounded by one outer torus (solid lines) and one inner torus (dashed lines) which defines the forbidden domain (hatched domain). (b) In the homoclinic situation, the inner bounding torus is reduced to a singular circle (dashed circle).

The last case is produced by the jerk conservative system introduced by [Sprott, 1997]. It is a metastable chaos since the invariant set is bounded by an unstable manifold connected to the origin of the state space which ejects the trajectory to infinity. This is a toroidal chaos $C^1T_d^2$, of a type which is similar to the toroidal chaos C^1T^2 produced by the Hénon-Heiles system [Table 1(g)], but here degenerated. Another particularity, possibly imposed by the inversion symmetry, is that the invariant set is bounded by a non-trivial genus-3 torus, the focus hole ($y = z = 0$) crossing the saddle hole ($x = y = 0$) (Fig. 6). Showing that such a bounding torus is of genus 3 is detailed by [Letellier & Gilmore, 2009]. This type of chaos must be therefore be investigated with a 2-component Poincaré section as plotted in Table 1(d).

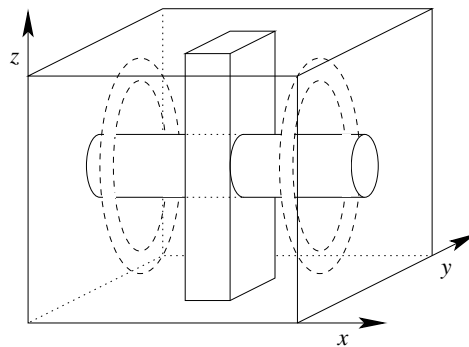


Figure 6. Bounding torus for the chaotic sea produced by the conservative jerk system (g). The two holes are organized as a crux: this is a genus-3 bounding torus. There is two inner trivial bounding tori (dashed lines). Parameter value: $a = 0.027$.

4. Complete treatment of the Rössler and Lorenz attractors

In this Section, we fully describe three different taxa. Let us start with the Rössler spiral attractor as plotted in Table 1(b). The spiral Rössler attractor is topologically described by the branched manifold shown in Fig. 1(a) when the Rössler system is rewritten in the space $\mathbb{R}^3(X, Y, Z)$ with $X = y$, $Y = x$, and $Z = z$ [Letellier, 2021]. This branched manifold is drawn according to the standard insertion introduced by [Tuffillaro *et al.*, 1992]: they are joined from the back to the front, and from the left to the right (Fig. 7). This avoids to use a second matrix to encode the insertion as used by [Gilmore, 1998; Gilmore & Lefranc, 2003]. Strips are labelled 0 and 1, from the center of the attractor to its periphery and according to the natural order [Bai-Lin, 1989]. The symbols are also chosen with respect to the parity of the strip: an even (odd) integer for an order preserving (reversing) strip. The strips are joined and squeezed at the thick line corresponding to the ideal location of the Poincaré section of the attractor.

The part of the branched manifold between the splitting chart and the joining chart is called a *linker* [Rosalie & Letellier, 2013] and can be described by a linking matrix reading as [Tuffillaro *et al.*, 1992; Letellier *et al.*, 1995; Rosalie & Letellier, 2013]

$$\mathcal{L}_R = \begin{bmatrix} 0 & 0 \\ 0 & +1 \end{bmatrix} \quad (6)$$

where element L_{ii} corresponds to the local torsion (the number of π -twists) of the i th strip. In the present case, they are $L_{00} = 0$ and $L_{11} = +1$ as drawn in Fig. 7. The off-diagonal element L_{ij} ($i \neq j$), corresponds to the permutation between the i th and the j th branches. By construction, the matrix is symmetric. The left bracket corresponds to the splitting chart and the double bracket to the joining chart [Rosalie & Letellier, 2013]. From this linking matrix and the orbital sequence designating periodic orbits, there is an algorithm to compute the linking number which quantifies the number of times one orbit circles another one (see [Le Sceller *et al.*, 1994; Letellier, 1994; Letellier *et al.*, 1995] for details). When the linking numbers computed from the periodic orbits numerically extracted from the attractor are equal to those algebraically computed from the linker (6), the branched manifold is validated and the topological characterization is completed.

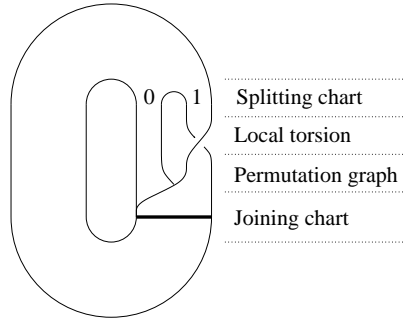


Figure 7. The branched manifold corresponding to the spiral Rössler attractor plotted in the space $\mathbb{R}^3(X, Y, Z)$.

The Lorenz attractor is bounded by the genus-3 torus drawn in Fig. 2(b) [Letellier *et al.*, 2005]. The Poincaré section is therefore made of the two-components Poincaré section

$$\mathcal{P}_{\pm} \equiv \left\{ (y_n, z_n) \in \mathbb{R}^2 \mid x_n = \pm \sqrt{b(R-1)}, \dot{x}_n \lesseqgtr 0 \right\}. \quad (7)$$

Normalizing these two components in the interval $]-1, 0[$ and $]0, +1[$, respectively, to construct the variable ρ , a four branch first-return map is obtained [Fig. 8(a)] [Byrne *et al.*, 2004]. According to this map, the branches are ordered according to

$$\bar{0} \triangleleft \bar{1} \triangleleft 0 \triangleleft 1.$$

Since the attractor is bounded by a genus-3 torus, there is two joining charts (one per component of the Poincaré section). The branched manifold is drawn in Fig. 8(b). It can be described by a double linker

$$\mathcal{L}_L = \begin{bmatrix} 0 & 0 & \cdot & \cdot \\ \cdot & +1 & 0 & 0 \\ \cdot & \cdot & 0 & 0 \\ 0 & 0 & \cdot & +1 \end{bmatrix} \quad (8)$$

where “.” means that the i th and the j th strips do not come from the same splitting graph and, consequently, cannot be permuted; it also means that the i th strip cannot be reinjected into the j th strip as checked with the Markov transition matrix

$$M_{ij} = \begin{bmatrix} 0.60 & 0.40 & 0 & 0 \\ 0 & 0 & 0.53 & 0.47 \\ 0 & 0 & 0.60 & 0.40 \\ 0.53 & 0.47 & 0 & 0 \end{bmatrix}, \quad (9)$$

a feature which is only valid for $i \neq j$ since, for instance, strip $\bar{1}$ is not reinjected in itself. Notice that we make a difference between “not permuted” ($L_{ij} = 0$) and “cannot be permuted” ($L_{ij} = \cdot$): in the former case, strips are in the same permutation chart but are not permuted while, in the latter, strips do not belong to the same permutation chart.

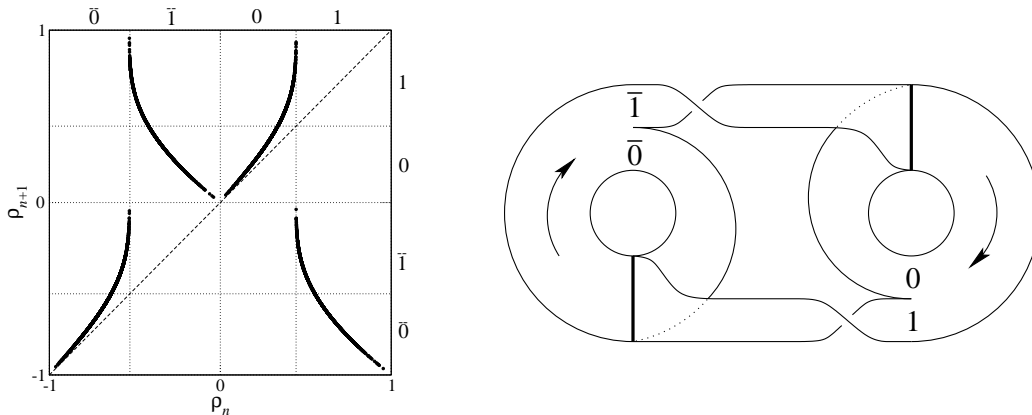


Figure 8. (a) First-return map to the two-component Poincaré section of the Lorenz attractor and (b) its description by a branched manifold. Parameter values: $R = 28$, $\sigma = 10$, and $b = \frac{8}{3}$.

The linker (8) thus encodes also the transition matrix between the different strips of the branched manifold: non-removed elements L_{ij} indicate that the transition from the i th strip to j th strip is possible (even when $L_{ij} = 0 \neq \cdot$). For multi-component attractor, the linker is thus no longer symmetric. As developed by [Le Sceller *et al.*, 1994] for one-component attractor, it is still possible to algebraically compute linking number from a multi-component linker. The difference occurs in the joining graph: for a $(g - 1)$ component attractor, there is $(g - 1)$ joining graphs to construct as it will be detailed in the example of the two orbits $(1\bar{0}\bar{1})$ and $(1\bar{0}\bar{1}\bar{0})$ (Fig. 9) as follows.

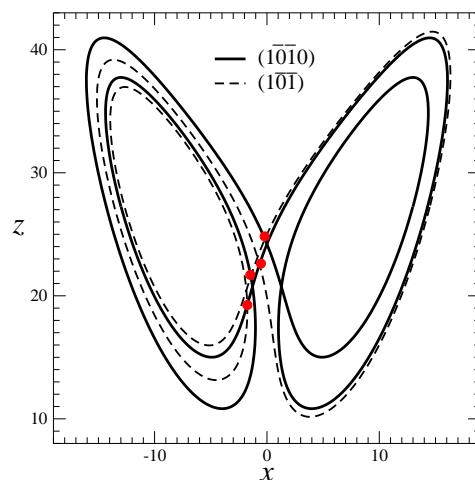


Figure 9. Periodic orbits $(1\bar{0}\bar{1})$ and $(1\bar{0}\bar{1}\bar{0})$ extracted from the Lorenz attractor. Four positive crossings (red disks) are counted between these two orbits.

Let us start with the numerical extraction of these two orbits. The oriented crossings are extracted with the third coordinate (see [Letellier *et al.*, 1995; Letellier, 2021] for details). Four positive crossings are counted: the linking number between these two periodic orbits is thus

$$L_k(1\bar{0}\bar{1}, 1\bar{0}\bar{1}\bar{0}) = +\frac{4}{2} = +2. \quad (10)$$

Extrapolating the original procedure [Le Sceller *et al.*, 1994], the linking number is predicted from the

linker (8) by

$$L_k(1\bar{0}\bar{1}, 1\bar{0}\bar{1}0) = + \frac{L_{11} + L_{\bar{1}\bar{1}} + 2L_{1\bar{1}} + L_{\bar{1}0} + 2L_{1\bar{0}} + L_{0\bar{0}} + L_{\bar{0}\bar{0}} + N_{\text{join}}^1 + N_{\text{join}}^2}{2} \quad (11)$$

where the three terms $2L_{\bar{0}\bar{1}}$, $L_{0\bar{0}}$ and $L_{\bar{0}\bar{0}}$ are removed since associated with a “.” in the linker (8). The joining graphs are constructed as follows. Let us start with the joining chart between strips $\bar{0}$ and 1. This graph is constructed between the periodic points $\bar{0}\bar{1}1$ and $1\bar{0}\bar{1}$ from the period-3 orbit, and from $\bar{0}\bar{1}01$ and $1\bar{0}\bar{1}0$ from the period-4 orbit (the first symbol indicates the strip in which the periodic point is located). First, these points are ordered according to the kneading theory [Bai-Lin, 1989; Letellier *et al.*, 1995; Letellier, 1994] as

$$\bar{0}\bar{1}0 \triangleleft \bar{0}\bar{1}01 \triangleleft 1\bar{0}\bar{1} \triangleleft 1\bar{0}\bar{1}0.$$

Then, according to [Le Sceller *et al.*, 1994], the points $1\bar{0}\bar{1}$ and $1\bar{0}\bar{1}0$ are inverted since belonging to an odd strip. Points from strips $\bar{0}$ and 1 are not permuted in block since they come from strips issued from two different splitting charts [Fig. 8(b)], that is, from strip which cannot be permuted. The upper row of the joining chart is thus

$$\bar{0}\bar{1}0 \triangleleft \bar{0}\bar{1}01 \triangleleft 1\bar{0}\bar{1}0 \triangleleft 1\bar{0}\bar{1}.$$

The lower row is made of the iterate of the previous points under a Bernoulli shift. These periodic sequences are then ordered according to the kneading theory, leading to

$$\bar{0}\bar{1}0 \triangleleft \bar{0}\bar{1}01 \triangleleft \bar{1}1\bar{0} \triangleleft \bar{1}01\bar{0}.$$

It remains to link the sequences related by a Bernoulli shift as shown in Fig. 10(a) and to count the crossings which are necessarily positive [Le Sceller *et al.*, 1994]. We thus find $N_{\text{join}}^1 = +2$. Proceeding in a similar way with strips $\bar{1}$ and 0, we get $N_{\text{join}}^2 = 0$ [Fig. 10(b)]. The linking number is thus

$$L_k(1\bar{0}\bar{1}, 1\bar{0}\bar{1}0) = \frac{+1 + 1 + 0 + 0 + 0 + 0 + 0 + 2 + 0}{2} = +2. \quad (12)$$

Counted and predicted linking numbers are thus equal. The here proposed procedure for multi-component attractor is thus validated.

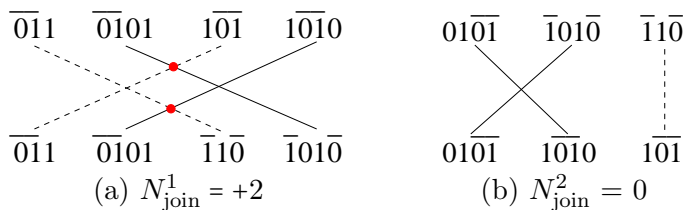


Figure 10. The two joining graphs, one for each component of the Poincaré section, between the two orbits ($1\bar{0}\bar{1}$) and ($1\bar{0}\bar{1}0$).

When the symmetry of the Lorenz system is removed, the attractor is characterized by $m = 1$, $p = 1$, $g = 1$, $n_c = 1$ and a branched manifold as shown in Fig. 7 (see [Letellier, 2021] for details). The single difference is that the folding of the Rössler attractor is replaced with a tearing [Byrne *et al.*, 2004]. Since the bifurcation diagram induced by a tearing is very different from the one obtained with a folding (a Logistic map) [Gilmore, 2015], they have to be distinguished as two different taxa. As developed by [Gilmore & Letellier, 2007], different taxa can be easily developed from a known one but with various symmetries.

5. Conclusion

After more than a half century of scientific researches with computers, a plethora of chaotic attractors are today found in the literature. In spite of this, what makes them specific was not yet very clear and, commonly, their characterization is limited to the spectrum of Lyapunov exponents, the first two taxonomic ranks according to our views. With the taxonomy here developed, we provided some guidelines to complete a full

characterization of chaotic attractors. We incorporated bounding tori as the third taxonomic rank: if this is quite easy for more three-dimensional chaos, determining bounding tori for higher-dimensional dynamics appears as an open problem in many cases. We left for future works the promising results obtained with the Betti numbers and their extension [Charó *et al.*, 2020, 2021].

Even worse is the problem related to the modality defined by the number of mixing processes in action in a given dynamics. If, for strongly dissipative three-dimensional systems, this is simply quantified with the number of monotone branches in first-return map, this is a complex problem for weakly dissipative systems and nearly never addressed for conservative systems. This is in fact deeply connected to the question of finding a generating partition for conservative dynamics [Christiansen & Politi, 1995]. The last taxonomic rank is associated with the topological description of the structure underlying the invariant set. We left untouched this last rank, mostly because this is still an open problem for most of toroidal chaos, in spite of the recent success for two simple cases [Mangiarotti & Letellier, 2021].

In spite of all of these problems, the taxonomy we here propose provides already a systematic labeling for every type of dynamical regimes based on two integers, intimately related to the number of positive and null Lyapunov exponents, respectively. This is a first efficient classification of chaotic regimes. Determining if the dynamics is degenerated and/or conjugated is also an important additional clue, showing that the Lyapunov exponents are not always sufficient to identify correctly the type of chaos. Clearly the role of bounding tori is fundamental in such a taxonomy and deserves to be better promoted. Hopefully, this taxonomy will stimulate dynamicists to go deeper in their analysis of the observed behaviors. One of the important lessons brought by this study is to show that characterizing chaotic attractors is still in its infancy. This taxonomy provides some guidelines for developing this area of research.

Acknowledgments

C. L. wishes to thank Jean-Marc Malasoma for stimulating discussions. N. S. thanks Igor Sataev and Vyacheslav Kruglov for fruitful discussion and the Russian Foundation for Basic Research for financial support of her work (grant No. 19-31-60030).

References

- Anishchenko, V. S. & Nikolaev, S. M. [2005] “Generator of quasi-periodic oscillations featuring two-dimensional torus doubling bifurcations,” *Technical Physics Letters* **31**, 853–855, doi:10.1134/1.2121837.
- Arnéodo, A., Couillet, P. H. & Spiegel, E. A. [1983] “Cascade of period doublings of tori,” *Physics Letters A* **94**, 1 – 6, doi:10.1016/0375-9601(83)90272-4.
- Aziz-Alaoui, M. A. [1999] “Differential equations with multispiral attractors,” *International Journal of Bifurcation & Chaos* **9**, 1009–1039, doi:10.1142/S0218127499000729.
- Bai-Lin, H. [1989] *Elementary symbolic dynamics and chaos in dissipative systems* (World Scientific Publishing, Singapore).
- Birkhoff, G. D. [1927] *Dynamical Systems* (American Mathematical Society, New York).
- Byrne, G., Gilmore, R. & Letellier, C. [2004] “Distinguishing between folding and tearing mechanisms in strange attractors,” *Physical Review E* **70**, 056214, doi:10.1103/PhysRevE.70.056214.
- Charó, G. D., Artana, G. & Sciamarella, D. [2020] “Topology of dynamical reconstructions from Lagrangian data,” *Physica D* **405**, 132371, doi:10.1016/j.physd.2020.132371.
- Charó, G. D., Artana, G. & Sciamarella, D. [2021] “Topological colouring of fluid particles unravels finite-time coherent sets,” *Journal of Fluid Mechanics* **923**, A17, doi:10.1017/jfm.2021.561.
- Charó, G. D., Sciamarella, D., Mangiarotti, S., Artana, G. & Letellier, C. [2019] “Equivalence between the unsteady double-gyre system and a 4D autonomous conservative chaotic system,” *Chaos* **29**, 123126, doi:10.1063/1.5120625.
- Christiansen, F. & Politi, A. [1995] “Generating partition for the standard map,” *Physical Review E* **51**, R3811–R3814, doi:10.1103/PhysRevE.51.R3811.

- Curry, J. & Yorke, J. A. [1978] “A transition from Hopf bifurcation to chaos: computer experiments with maps on \mathbb{R}^2 ,” *Lecture Notes in Mathematics* **668**, 48–66.
- Ereshefsky, M. [2000] *The Poverty of the Linnaean Hierarchy: A Philosophical Study of Biological Taxonomy*, Cambridge Studies in Philosophy and Biology (Cambridge University Press, Cambridge), doi:10.1017/CBO9780511498459.
- Franceschini, V. [1983] “Bifurcations of tori and phase locking in a dissipative system of differential equations,” *Physica D* **6**, 285–304, doi:10.1016/0167-2789(83)90013-1.
- Frederickson, P., Kaplan, J. L., Yorke, E. D. & Yorke, J. A. [1983] “The Lyapunov dimension of strange attractors,” *Journal of Differential Equations* **49**, 185–207, doi:10.1016/0022-0396(83)90011-6.
- Gilmore, R. [1998] “Topological analysis of chaotic dynamical systems,” *Reviews of Modern Physics* **70**, 1455–1529, doi:10.1103/RevModPhys.70.1455.
- Gilmore, R. [2015] “Explosions in Lorenz maps,” *Chaos, Solitons & Fractals* **76**, 130–140.
- Gilmore, R. & Lefranc, M. [2003] *The topology of chaos* (Wiley), ISBN 9780471408161, doi:10.1002/9783527617319.
- Gilmore, R. & Letellier, C. [2007] *The symmetry of chaos* (Oxford University Press, New York).
- Grebogi, C., Ott, E., Pelikan, S. & Yorke, J. A. [1984] “Strange attractors that are not chaotic,” *Physica D* **13**, 261–268.
- Hénon, M. & Heiles, C. [1964] “The applicability of the third integral of motion: some numerical experiments,” *The astronomical Journal* **69**, 73–79.
- Kaneko, K. [1983] “Doubling of torus,” *Progress of Theoretical Physics* **69**, 1806–1810, doi:10.1143/PTP.69.1806.
- Kaneko, K. [1986] *Collapse of tori and genesis of chaos in dissipative systems* (World Scientific Publishing, Singapore).
- Kaplan, J. & Yorke, J. [1979] “Chaotic behavior of multidimensional difference equations,” *Lecture Notes in Mathematics* **730**, 204–227.
- Klein, F. [1882] *Über Riemann’s Theorie der algebraischen Functionen und ihrer Integrale* (Druck und Verlag von B. G. Teubner, Leipzig).
- Klein, M. & Baier, G. [1991] “Hierarchies of dynamical systems,” *A chaotic hierarchy* (World Scientific Publishing), pp. 1–24.
- Le Sceller, L., Letellier, C. & Gouesbet, G. [1994] “Algebraic evaluation of linking numbers of unstable periodic orbits in chaotic attractors,” *Physical Review E* **49**, 4693–4695, doi:10.1103/PhysRevE.49.4693.
- Letellier, C. [1994] “Caractérisation topologique et reconstruction des attracteurs étranges,” PhD thesis, University of Paris VII, Paris, France, doi:10.13140/RG.2.1.1280.5281.
- Letellier, C. [2021] “Branched manifolds for the three types of unimodal maps,” *Communications in Non-linear Science and Numerical Simulation* **101**, 105869, doi:10.1016/j.cnsns.2021.105869.
- Letellier, C. & Aguirre, L. A. [2012] “Required criteria for recognizing new types of chaos: Application to the “cord” attractor,” *Physical Review E* **85**, 036204.
- Letellier, C., Bennoud, M. & Martel, G. [2007] “Intermittency and period-doubling cascade on tori in a bimode laser model,” *Chaos, Solitons & Fractals* **33**, 782–794, doi:10.1016/j.chaos.2006.01.109.
- Letellier, C., Dutertre, P. & Gouesbet, G. [1994] “Characterization of the Lorenz system, taking into account the equivariance of the vector field,” *Physical Review E* **49**, 3492–3495, doi:10.1103/PhysRevE.49.3492.
- Letellier, C., Dutertre, P. & Maheu, B. [1995] “Unstable periodic orbits and templates of the Rössler system: Toward a systematic topological characterization,” *Chaos* **5**, 271–282, doi:10.1063/1.166076.
- Letellier, C. & Gilmore, R. [2001] “Covering dynamical systems: Two-fold covers,” *Physical Review E* **63**, 016206, doi:10.1103/PhysRevE.63.016206.
- Letellier, C. & Gilmore, R. [2009] “Poincaré sections for a new three-dimensional toroidal attractor,” *Journal of Physics A* **42**, 015101.
- Letellier, C. & Gouesbet, G. [1995] “Topological characterization of a system with high-order symmetries: the proto-Lorenz system,” *Physical Review E* **52**, 4754–4761.
- Letellier, C. & Rössler, O. E. [2020] “An updated hierarchy of chaos,” *Chaos: The world of nonperiodic*

- oscillations* (Springer, Cham, Switzerland), pp. 181–203, doi:10.1007/978-3-030-44305-4.
- Letellier, C., Tsankov, T. D., Byrne, G. & Gilmore, R. [2005] “Large-scale structural reorganization of strange attractors,” *Physical Review E* **72**, 026212, doi:10.1103/PhysRevE.72.026212.
- Malykh, S., Bakhanova, Y., Kazakov, A., Pusuluri, K. & Shilnikov, A. [2020] “Homoclinic chaos in the Rössler model,” *Chaos* **30**, 113126, doi:10.1063/5.0026188.
- Mangiarotti, S. & Letellier, C. [2021] “Topological characterization of toroidal chaos: A branched manifold for the Deng toroidal attractor,” *Chaos* **31**, 013129, doi:10.1063/5.0025924.
- Ménard, O., Letellier, C., Maquet, J., Sceller, L. L. & Gouesbet, G. [2000] “Analysis of a non synchronized sinusoidally driven dynamical system,” *International Journal of Bifurcation & Chaos* **10**, 1759–1772.
- Mindlin, G. M. & Gilmore, R. [1992] “Topological analysis and synthesis of chaotic time series,” *Physica D* **58**, 229–242, doi:10.1016/0167-2789(92)90111-Y.
- Miranda, R. & Stone, E. [1993] “The proto-Lorenz system,” *Physics Letters A* **178**, 105–113.
- Parker, T. S. & Chua, L. O. [1989] *Practical numerical algorithms for chaotic systems* (Springer Verlag, Berlin–New York).
- Rosalie, M. & Letellier, C. [2013] “Systematic template extraction from chaotic attractors: I. Genus-one attractors with an inversion symmetry,” *Journal of Physics A* **46**, 375101, doi:10.1088/1751-8113/46/37/375101.
- Rössler, O. E. [1976] “An equation for continuous chaos,” *Physics Letters A* **57**, 397–398, doi:10.1016/0375-9601(76)90101-8.
- Rössler, O. E. [1978] “The hierarchy of chaos,” *10th Summer Seminar on Applied Mathematics*, F. C. Hoppensteadt (organizer), University of Utah.
- Rössler, O. E. [1979a] “Continuous chaos: four prototype equations,” *Annals of the New York Academy of Sciences* **316**, 376–392.
- Rössler, O. E. [1979b] “An equation for hyperchaos,” *Physics Letters A* **71**, 155–157.
- Rössler, O. E. [1983] “The chaotic hierarchy,” *Zeitschrift für Naturforschung A* **38**, 788–801.
- Ruelle, D. & Takens, F. [1971] “On the nature of turbulence,” *Communications in Mathematical Physics* **20**, 167–192.
- Séquin, C. H. [2013] “On the number of Klein bottle types,” *Journal of Mathematics and the Arts* **7**, 51–63, doi:10.1080/17513472.2013.795883.
- Sprott, J. C. [1997] “Some simple chaotic jerk functions,” *American Journal of Physics* **65**, 537–543, doi:10.1119/1.18585.
- Sprott, J. C. [2011] “A proposed standard for the publication of new chaotic systems,” *International Journal of Bifurcation & Chaos* **21**, 2391–2394, doi:10.1142/S021812741103009X.
- Stankevich, N. V., Shchegoleva, N. A., Sataev, I. R. & Kuznetsov, A. P. [2020] “Three-dimensional torus breakdown and chaos with two zero Lyapunov exponents in coupled radio-physical generators,” *Journal of Computational and Nonlinear Dynamics* **15**, 111001.
- Tricoche, X., Garth, C. & Sanderson, A. [2011] “Visualization of topological structures in area-preserving maps,” *IEEE Transactions on Visualization and Computer Graphics* **17**, 1765–1774, doi:10.1109/TVCG.2011.254.
- Tsankov, T. D. & Gilmore, R. [2003] “Strange attractors are classified by bounding tori,” *Physical Review Letters* **91**, 134104.
- Tsankov, T. D. & Gilmore, R. [2004] “Topological aspects of the structure of chaotic attractors in \mathbb{R}^3 ,” *Physical Review E* **69**, 056206.
- Tufillaro, N. B., Abbott, T. & Reilly, J. [1992] *An experimental approach to nonlinear dynamics and chaos* (Addison-Wesley, Redwood City, CA), ISBN 9780201554410.
- Ueda, Y. [1993] *The Road to Chaos*, Science frontier express series (Aerial Press, Santa Cruz, CA), ISBN 9780942344141.